


## Article

# Microwave-Assisted Synthesis of Luminescent Carbonaceous Nanoparticles as Silkworm Feed for Fabricating Fluorescent Silkworm Silk

Wenkai Chen <sup>1</sup>, Yangsheng Zhong <sup>1</sup>, Gangrong Fu <sup>2</sup> , Wenxuan Lai <sup>1</sup>, Ziwen Pan <sup>1</sup>, Yulian Yang <sup>1</sup>, Fangyan Chen <sup>1,\*</sup> and Huichao Yan <sup>1,\*</sup>

<sup>1</sup> College of Animal Science, South China Agricultural University, Guangzhou 510000, China

<sup>2</sup> College of Engineering, Jiangxi Agricultural University, Nanchang 330045, China

\* Correspondence: chenfangyan@scau.edu.cn (F.C.); yanhc@scau.edu.cn (H.Y.)

**Abstract:** In biomedical engineering, optics, and photonics, fluorescent silkworm silk has many potential applications, but its complex preparation process and the environmental pollution of corresponding chemical dyeing methods hinder its development. Herein, we provide a green and effective method for fabricating fluorescent silkworm silk with enhanced mechanical properties. Citric acid and urea were selected as raw materials for synthesizing carbon dots (CDs), which were applied as additives of silkworm feed to produce fluorescent silkworm silks by microwave-assisted methods. The results showed that a diet of mulberry leaf with 0.5 wt% CDs was safe for silkworms and did not affect silk yield. CDs rapidly entered silkworms and accumulated in their blood and silk glands. After feeding for 90 min, the silk gland fluorescence appeared prominent. Compared with ordinary silk, the highest elongation at break of the CD-modified silk was 22.24%, and the breaking strength was 28.07 MPa, which were increases of 5.05 and 22.84%, respectively. The CD-modified silk displayed intrinsic blue fluorescence when exposed to a 405 nm laser, exhibited no cytotoxic effect on L929 cells and had excellent cell adhesion. The strategy proposed in this work is not only environmentally friendly but can also produce high-quality fluorescent silk on a large scale.



**Citation:** Chen, W.; Zhong, Y.; Fu, G.; Lai, W.; Pan, Z.; Yang, Y.; Chen, F.; Yan, H. Microwave-Assisted Synthesis of Luminescent Carbonaceous Nanoparticles as Silkworm Feed for Fabricating Fluorescent Silkworm Silk. *Coatings* **2023**, *13*, 31. <https://doi.org/10.3390/coatings13010031>

Academic Editor: Kuthati Yaswanth

Received: 24 November 2022

Revised: 19 December 2022

Accepted: 21 December 2022

Published: 24 December 2022



**Copyright:** © 2022 by the authors. Licensee MDPI, Basel, Switzerland. This article is an open access article distributed under the terms and conditions of the Creative Commons Attribution (CC BY) license (<https://creativecommons.org/licenses/by/4.0/>).

**Keywords:** silkworm silk; carbon dots; fluorescent silk; mechanical properties; feeding method; toxicity

## 1. Introduction

As a natural filament fiber, silkworm silk has been used for thousands of years. In traditional textile production, due to its excellent mechanical properties, it is widely used [1]. However, with the continuous development of chemical technology, artificial synthetic fibers that can imitate the appearance and characteristics of natural silk fibers are now being produced. Synthetic fibers continue to occupy and expand the market, resulting in great challenges for traditional silk products. To improve the performance of silkworm silk and expand its functions and applications, many researchers have been devoted to the functional modification of silk. For example, silkworms were fed organic colored matter to produce colored silk [2,3], their genes were modified to acquire fluorescent silk [4], silk fibroin was regenerated to obtain bioactive biomaterials [5,6], and silk was processed with chemical or physical methods to obtain multifunctional silk [7,8].

Fluorescent silk will be essential for developing tissue engineering scaffolds in the future [9]. Unfortunately, natural silk has almost no fluorescence. A variety of exogenous postprocessing techniques have been used to successfully prepare functional fluorescent silk, such as combining quantum dots (QDs) [10,11], metal nanoclusters [12,13], and organic dyes [14,15] combined with silkworm silk by chemical or physical means. However, most of these techniques inevitably require harsh postprocessing conditions and complex procedures and are not environmentally friendly. In addition, the stability of the fluorescent substance bound to silk is still a problem. Gene engineering technology for preparing

fluorescent silk is indeed a feasible method [16], but it is expensive, inefficient, and complicated to operate. Studies have shown that feeding silkworms with dye-containing feed can directly produce natural fluorescent silk [17,18]. Compared with the above two methods, the feeding method is a significant improvement in convenience and is friendly to the environment, conducive to large-scale production and can allow the modification of silk properties at the source. An innovative class of fluorescent nanomaterials, carbon dots (CDs) have outstanding biocompatibility and superior fluorescence properties [19]. Moreover, a large number of CDs are manufactured from biomass, so they are bio-safe, low-priced, and environmentally friendly [20]. Compared with fluorescent organic dyes, rare earth nanoparticles and semiconductor QDs, CDs have better mechanical properties, higher brightness and light stability, and lower toxicity, making them ideal for feeding silkworms [21]. In addition, as a nanodye, CDs disperse evenly in the diet, promoting *in vivo* uptake to form high-quality silk [17]. Blue-emitting CDs were earlier used to feed silkworms in 2019 and produced intrinsically fluorescent silkworm silk [17]. The same year, feeding blue-emitting CDs, CdSe/ZnS QDs and rhodamine to silkworms produced blue, green and red fluorescent composite silk, respectively [18]. The biosafety of CdSe/ZnS QDs is a thorny issue due to their potential cytotoxicity.

Hydrothermal and microwave-assisted methods are commonly used for the synthesis of CDs. The hydrothermal method is a method to prepare CDs by mixing the carbon source and water or organic solvent and then transferring them to a reaction vessel, which is heated to produce high temperature and pressure in the reaction vessel [22]. The microwave-assisted method is a synthesis method that uses microwaves to provide reaction heat [23], and the greatest advantage is that it can provide precise, intensive, and uniform energy to the reaction system, thus compensating for the low efficiency of CD synthesis and undesirable physical and chemical properties caused by the traditional hydrothermal method due to uneven heating, strict experimental conditions and long reaction time. In recent years, many researchers have applied microwave-assisted methods to the synthesis of CDs [24], using the microwave method to synthesize multicolor fluorescent CDs in only 14 min, which greatly saves the synthesis time compared with the traditional hydrothermal method. The microwave-assisted method can rapidly and efficiently convert biomass into functional nanomaterials. Therefore, in this study, citric acid/urea CDs (CA/U-CDs) were synthesized by the microwave-assisted method using citric acid and urea as raw materials.

Mulberry silkworms are an economic insect sensitive to the environment. The mulberry silkworm variety “9 Fu × 7 Xiang” is a major production variety fed widely in South China. We fed mulberry silkworms of the “9 Fu × 7 Xiang” variety with different doses of CA/U-CDs during the period from the second day of the fifth instar until silkworms matured to produce fluorescent silk. Firstly, the safety of CDs for silkworms was evaluated by the silkworms’ growth, the quality of the cocoons and the morphology of silk glands. Further, we also preliminarily explored the absorption, metabolism of CA/U-CDs in silkworms, and the accumulation and distribution in silk glands. Finally, the fluorescent and mechanical properties of silk fibroin fiber were analyzed. The cytotoxic effect on L929 cells of CD-modified silk was evaluated. This study would provide a basis for the large-scale production of fluorescent silk in South China, as well as references for tissue engineering applications.

## 2. Materials and Methods

### 2.1. Preparation of CDs

CA and urea were used as the carbon source and surface passivation agent, respectively [19]. Under microwave-assisted conditions, these two components were mixed in H<sub>2</sub>O and heated at 750 W for 4 min. We dissolved 3.0 g of CA and 2.0 g of urea with 10 mL of distilled water. After heating the mixture in a domestic microwave oven for 4 min, the colorless solution transformed into a reddish-brown solid, indicating CD formation. A minimum amount of distilled water was used to dissolve the resulting solid and centrifuged (8000 rpm) for 10 min. Furthermore, using a dialysis bag (molecular weight cutoff:

1000 Da), the brown supernatant was dialyzed in distilled water for 2 days to remove low-molecular-weight impurities. Finally, the purified products (inside the dialysis bags) were lyophilized and collected for further use.

## 2.2. CD Characterization Technique

Transmission electron microscopy (TEM) and high-resolution transmission electron microscopy (HRTEM) images were collected using a JEM-2100 transmission electron microscope (JEM-2100, JEOL, Tokyo, Japan). A Shimadzu UV-2550 spectrophotometer was used to record the UV–vis absorption spectra. Fluorescence spectra curves were recorded with a fluorescence spectrofluorometer (F-7000, Hitachi, Tokyo, Japan). Fourier transform infrared spectra (FT-IR) were measured using a Thermo Fisher Nicolet IS10 FT-IR spectrometer (Nicolet IS10, Thermo Fisher, Waltham, MA, USA).

## 2.3. Silkworm Feeding and Fluorescent Silk Production

Silkworms (9·Fu × 7·Xiang strain from China) were raised in a climatic chamber. All silkworms were fed fresh mulberry leaves until the second day of the fifth instar. A number of 200 silkworms were equally split into four groups: control, CDs-0.25%, CDs-0.5%, and CDs-0.75% groups, respectively. Then, we fed them regular mulberry leaves and mulberry leaves containing 0.25, 0.50 and 0.75 wt% CDs from the second day of the fifth instar until they had spun their cocoons. During the rearing period, we observed the apparent performance (mental state and activity of silkworms), weighed them daily, and recorded the survival rate. Mulberry leaves containing different doses of CDs were prepared by the following procedure. Firstly, CDs were weighed according to the mass fraction ratio of CDs/fresh mulberry leaves, and CDs were dissolved in the minimum amount of distilled water and sprayed on the surface of fresh mulberry leaves. Finally, they were dried naturally at room temperature. Note that before spraying on fresh mulberry leaves, all aqueous CD dispersions underwent a 20 min sonication process. The reeling of the silk from the cocoons was performed according to a previously reported method [25]. To produce silk fibroin fiber, the silk was degummed twice using a 0.5% (*w/v*) Na<sub>2</sub>CO<sub>3</sub> solution at 90 °C for 30 min each time. The silk was then thoroughly rinsed with deionized water and dried at 50 °C.

## 2.4. Paraffin Sectioning of Silkworm Tissue

Five silkworm larvae from each group were dissected right before cocooning on the sixth day of the fifth instar stage. The middle and posterior silk glands were fixed in a 4% paraformaldehyde solution, embedded in paraffin after being dehydrated with ethanol graded solutions from 70 to 100%, sliced to a thickness of 5 μm by a paraffin slicing machine, and stained with hematoxylin and eosin (H&E) for histopathologic analyses.

## 2.5. Fluorescence Imaging and Fluorescence Spectroscopy

The middle and posterior silk glands and blood obtained from silkworm from the control and CD groups were placed in a UVP gel imaging system (BIO-RAD, Richmond, CA, USA) for fluorescence imaging. After being excited by a 405 nm laser, photographs of the silk fibroin fiber were captured using confocal laser microscopy (ZEISS, LS M880, Oberkochen, Germany). The photoluminescence (PL) spectra of the middle, posterior silk glands and silk fibroin fiber were recorded after excitation with a 370 nm laser by using a Hitachi FL-7000 PL instrument.

## 2.6. Scanning Electron Microscopy

Using a scanning electron microscope, the silk fibroin fibers from each group were morphologically examined (ZEISS, EVO MA 15, Oberkochen, Germany). Each sample was given a 20 nm gold covering, and the microscope was operated at 10.0 kV. To observe the growth and proliferation of L929 cells on silk scaffolds by SEM, L929 cells seeded on scaffolds (L929 cells/silk scaffolds) were fixed in 1.0% osmic acid solution for 1 h. After

removing the osmic acid solution, and after further PBS washes, L929 cells/ silk scaffolds were dehydrated using a gradient of ethanol aqueous solutions (50, 70, 80, 90 and 100 vol%). Finally, the resulting L929 cells/silk scaffolds were treated in a mixture of ethanol and isoamyl acetate and then critical point-dried.

### 2.7. Mechanical Properties Measurement

The mechanical properties of silkworm silk were tested at 25 °C and 60% relative humidity with an MTS Industrial Systems (Shenzhen, China) 2 kN tensile testing machine at a constant crosshead speed of 10 mm/min. The experimental stress–strain curves were recorded to obtain the elongation at break and breaking strength.

### 2.8. FT-IR Spectroscopy

The secondary structure of silk fibroin fibers was analyzed by Fourier infrared spectroscopy (Nicolet IS10, Thermo Fisher, Waltham, MA, USA). The secondary structure of the silk fibroin fiber was quantified by studying the spectral region corresponding to the amide I band ( $1600\text{ cm}^{-1}$ – $1700\text{ cm}^{-1}$ ) and deconvoluting the amide I band in the IR spectrum using the software Peak Fit 4.0 [26].

### 2.9. Cell Culture

The CD-modified silk's biocompatibility was examined using mouse fibroblast L929 cells obtained from Procell Life Science & Technology Co., Ltd. The cells were propagated in Dulbecco's modified Eagle's medium (DMEM) with 10% fetal bovine serum added, and they were incubated in a CO<sub>2</sub> incubator at 5% CO<sub>2</sub>, 37 °C. Silk scaffolds were constructed by manually twining the silk fibroin fiber around a glass coverslip. After being repeatedly washed with phosphate-buffered saline (PBS), silk scaffolds were put in a 6-well plate and sterilized using a 75% (*v/v*) ethanol aqueous solution. They were seeded on scaffolds at a density of  $2 \times 10^5$  cells per well, and the L929 cells/silk scaffolds were incubated for 24 and 72 h at 37 °C in a humid environment with 5% CO<sub>2</sub>. Finally, the cell morphology was observed using an inverted microscope.

### 2.10. Flow Cytometry

We collected L929 cells that were cultured on inoculated silk scaffolds for 72 h. The cells were subjected to two PBS washes, resuspended in loading buffer and stained at room temperature with annexin V-APC and propidium iodide (PI) to identify cell apoptosis. The treated cells were immediately analyzed using a fluorescence-activated cell sorting (FACS) flow cytometer (BD, AccuriTMC6 plus, Franklin Lakes, NJ, USA).

### 2.11. Confocal Microscopy

Fluorescent pictures of cells on silk scaffolds were captured by laser confocal microscopy. The cells were planted and cultivated on the silk scaffolds for 72 h. The matrices were then washed two times with PBS to remove excess serum, followed by incubation in 4% paraformaldehyde for 10 min. The samples were permeabilized for 10 min at room temperature with 0.50% Triton X-100. The constructs were first stained with DAPI for 30 min at room temperature and then incubated with rhodamine–phalloidin solution for 30 min. Using a confocal laser scanning microscope, fluorescence pictures of stained constructs were captured (ZEISS, LS M880, Oberkochen, Germany). The laser wavelength of DAPI was 405 nm and that of rhodamine–phalloidin was 559 nm.

## 3. Results and Discussion

### 3.1. Structure and Properties of CDs

A straightforward one-step microwave-assisted method with anhydrous CA and urea was used to synthesize CDs. The CDs were first characterized by TEM. The TEM photographs confirmed that the resulting CDs had good dispersion in aqueous solution with an average particle size of approximately 2.8 nm (Figure 1a). The HRTEM images showed

0.24 nm lattice stripes, corresponding to the (1120) face of graphite (Figure 1b) [27,28]. Due to their size-limiting effect and photoluminescent properties, bright blue fluorescence was seen in the CD aqueous solution under excitation at 365 nm (Figure 1c). The PL emission spectra in Figure 1d show that when CDs were excited by a laser at wavelengths of 300–400 nm, their dilute solution exhibits a fluorescence emission centered at 467 nm, with an optimal excitation of 376 nm, which indicates that CDs can absorb UV light and convert it into blue light. The CDs' UV-vis spectra revealed an absorption at around 240 nm that is caused by the  $\pi$ - $\pi^*$  transition and a typical peak at about 380 nm that is attributed to the  $n$ - $\pi^*$  leap of C=O/C=N bond (Figure 1e) [29]. FT-IR was used to further investigate the chemical composition and structure of the synthesized CDs. According to Figure 1f, the broad absorption band at  $3442\text{ cm}^{-1}$  is attributed to the stretching vibrations of O-H and N-H bonds [30]. The absorption peak at  $2931\text{ cm}^{-1}$  is attributed to the stretching vibrations of -CH and -CH<sub>2</sub>, which represent hydrophobic long alkyl chains and aromatic rings [21,31]. The absorption peak at  $1688\text{ cm}^{-1}$  is ascribed to the C=O stretching vibration peak, and the absorption peak at  $1400$ – $1200\text{ cm}^{-1}$  is ascribed to the in-plane bending vibration of O-H and the tensile vibration of C-O, which indicates the presence of -COOH on the CD surface [32]. The FT-IR findings show that the CDs have an amphiphilic structure and the CD surface contains -OH, -COOH, -NH<sub>2</sub> and other abundant functional groups.

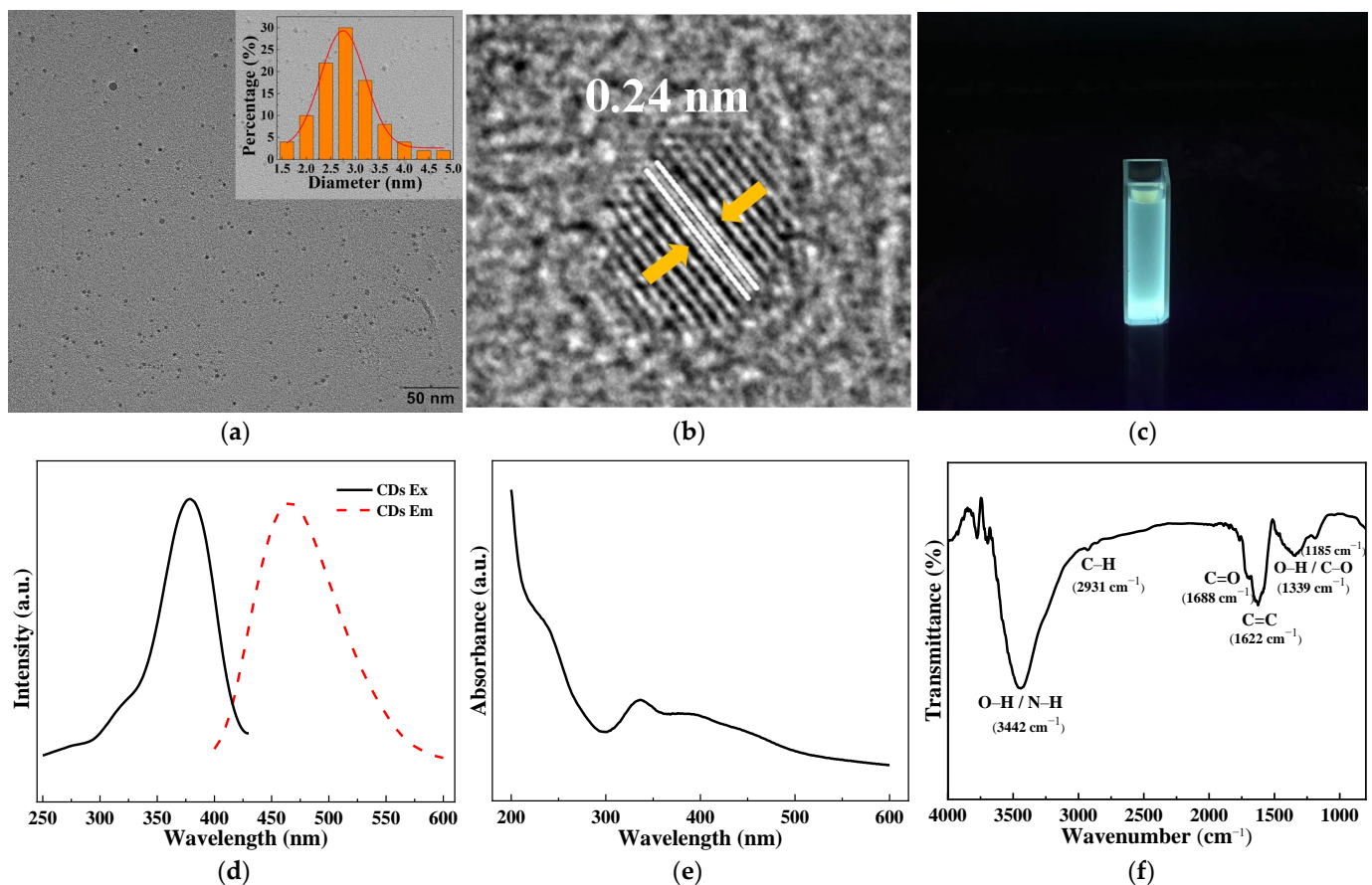


**Figure 1.** Characteristics of CDs. (a) TEM image of CDs (inset: particle size distribution); (b) HRTEM image of CDs; (c) photo of CD powder aqueous solution under 365 nm UV radiation; (d) PL spectra of CDs; (e) UV-vis spectra of CDs; (f) FT-IR spectra of CDs.

As typical renewable resources, CA and urea have many advantages, such as wide source, low price and high biosafety. In this work, compared with the raw material used by Zhang [17] for CD fabrication (synthesized from CA and ethylenediamine by a hydrothermal method), our raw materials were safer, and the synthesis process was

more rapid, cost-effective and sustainable. The resulting CDs had a small particle size (approximately 2.8 nm), good dispersion and amphiphilic structure, which is crucial for the feeding method. The nanosize and excellent dispersibility of CDs not only facilitates entry into the silk gland but also does not significantly affect the normal physiological activities of silkworms. In addition, the amphiphilic structure of CDs and the abundant –COOH and –OH groups on the surface can form hydrogen bonds with the amino groups of silk fibroin, producing high-quality silk. The nanosize, excellent fluorescent properties and amphiphilic structure of CDs are beneficial for feeding silkworms. Therefore, the CDs were used as additive substances to obtain fluorescent silkworm silk with enhanced mechanical properties.

### 3.2. Evaluation of the Safety of CDs for Silkworms

To investigate the safety of CDs for silkworms, the growth status of silkworms was first observed, and for each group, the average weight, growth rate and survival rate of the silkworm larvae were determined. Although these silkworm larvae were divided into four groups and fed different doses of CDs, all silkworm larvae were steadily in the fifth instar, and their weights increased from 0.61 to 2.31 g, with an average growth rate of 0.27 g/d (Figure 2a). Finally, each group's survival rate reached 95% (Figure 2b). These results preliminarily suggested that the modified diet was safe for silkworms.

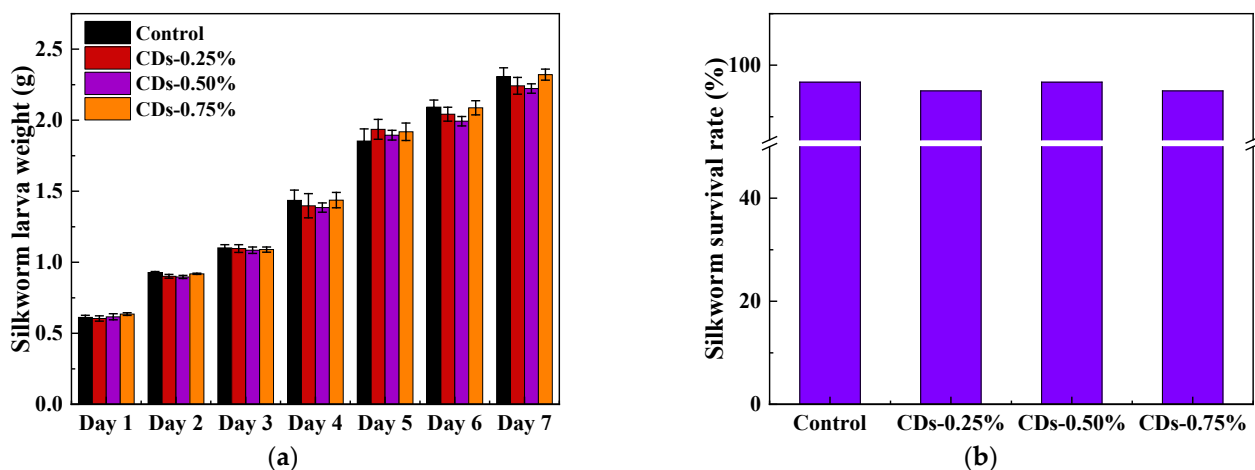


**Figure 2.** Effect of CDs on silkworm growth. (a) Weight of silkworm larvae from the first to the seventh day of the fifth instar. (b) Survival rate of silkworm larvae.

Silk glands are vital organs for silkworms to produce sericin and silk fibroin [33]. Therefore, we prepared H&E stained sections of silk glands to further analyze the effect of CDs on silkworm tissues. The silk gland mainly comprises the outer membrane, glandular cell layer and inner membrane. It is understood that the quantity of membrane vacuolization can be used to assess the degree of structural damage to the silk gland [34], where the vacuole is the structure surrounded by the epidermoid cell of the membrane [35]. According to Figure 3a,b, the silk gland of the control group had a complete morphology and the glandular cell layer was arranged neatly and densely. All CD groups had normal middle silk gland structures with thin walls and relatively full gland lumens, with no significant pathological changes (Figure 3a). However, the posterior silk glands of the CD groups had different degrees of vacuoles (Figure 3b, white arrows); the number of vacuoles in the posterior silk glands increased as the CD dose increased, especially in the CDs-0.75% group. This phenomenon may be due to the accumulation of CD particles mainly in the posterior silk glands [17]. From a biological point of view, nanoparticles are small enough to interact with the cells of living organisms. When exogenous nanoparticles enter an organism, the nanoparticle surface is immediately wrapped by biomolecules such as proteins, organic matter and enzymes, forming a new binding body called the protein crown [36]. A

nanobio interface is created between the biomolecules and nanoparticles, and this process affects protein synthesis and secretion to some extent. The high concentration of protein adsorbed on the nanoparticle surface can increase the partial unfolding of proteins, and the interactions between nanoparticles and proteins may also lead to protein agglomeration and the production of harmful products, such as amyloid deformation [37]. An irreversible change in protein structure is the main molecular mechanism causing the damage, which also explains the pathology of the posterior silk glands of the silkworm during the late feeding period.

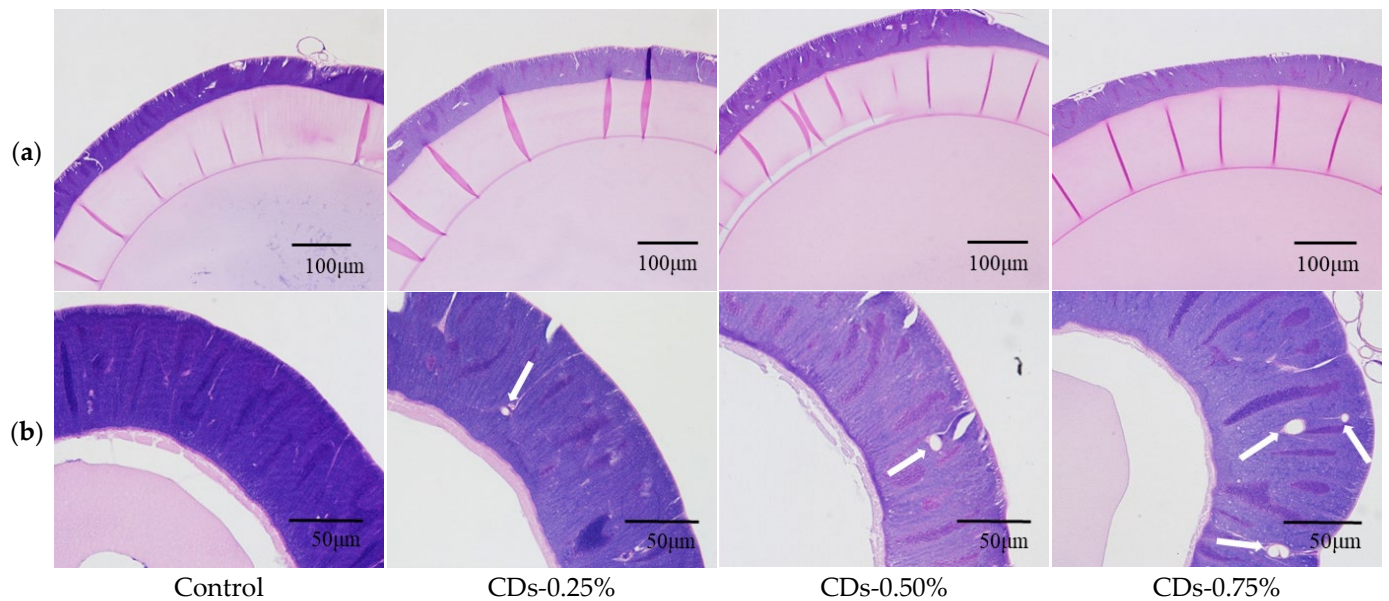


**Figure 3.** Histophysiological images of silkworms: (a) middle silk gland; (b) posterior silk gland. The white arrow points to the vacuoles in the posterior silk glands.

To investigate whether the vacuoles in the posterior silk glands could affect the silkworm spinning behavior, the silk yield of the silkworms was calculated, including the cocoon shape, cocoon mass, cocoon shell mass and the ratio of the cocoon shell. The cocoons of the control and CD groups were nearly the same size, with long oval shapes, white colors, irregular wrinkles on the surface and a natural luster (Figure 4). As shown in Table 1, the average weight of the cocoon mass in the CD groups was 0.87 to 0.90 g, which was close to that in the control group. The CD and control groups had almost the same cocoon shell mass (approximately 0.19–0.20 g). The cocoon shell ratio measures how much silk can be reeled from a specific number of young, fresh cocoons [38]. There was no discernible difference between the ratio of cocoon shell in the CD groups and the control group (approximately 21.74–22.61%). Therefore, it is assumed that the vacuoles in the posterior silk glands do not affect the spinning behavior and silk yield of silkworms. The above results indicated that the method reported in this work can be further applied to the production of functional silk. Although high doses of CDs could damage the silk glands of silkworms to a certain extent, the damage to the silk glands by CDs did not affect the growth and spinning behavior of silkworms and thus reduce the silk yield.

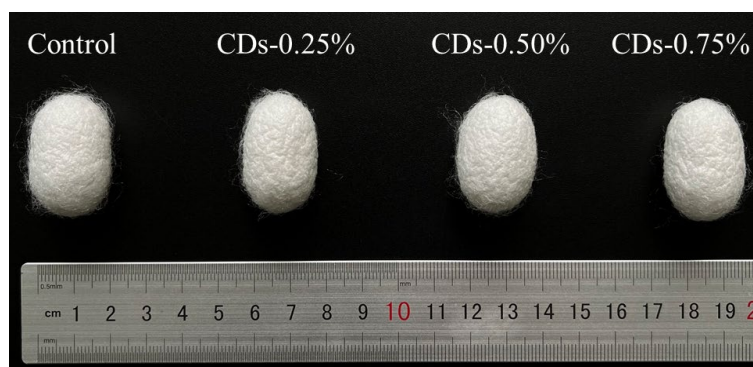


**Figure 4.** External appearance of the cocoons of the control and CD groups.

**Table 1.** Effect of CDs on the silk yield of silkworms.

-	Control	CDs-0.25%	CDs-0.50%	CDs-0.75%
Cocoon length (mm)	26.64 ± 1.58	27.12 ± 1.52	27.04 ± 1.52	26.93 ± 1.60
Cocoon width (mm)	14.66 ± 1.07	14.83 ± 0.65	14.73 ± 1.05	14.70 ± 0.74
Cocoon mass (g)	0.89 ± 0.05	0.89 ± 0.02	0.90 ± 0.02	0.87 ± 0.02
Cocoon shell mass (g)	0.20 ± 0.03	0.20 ± 0.01	0.19 ± 0.02	0.19 ± 0.01
Ratio of cocoon shell (%)	21.90 ± 0.52	22.61 ± 0.78	21.74 ± 1.01	21.95 ± 1.19

### 3.3. Accumulation and Distribution of CDs in the Silkworm Body

Shortening silkworm feeding cycle and improving the additive conversion efficiency are crucial for optimizing the feeding method. Thus, we dissected the silkworms at different points after feeding to investigate the CD uptake and distribution in silkworm tissues and the CD excretion, which will provide new ideas for optimizing the feeding cycle of additives. It was observed that the silkworm blood had a bright yellowish fluorescence after feeding silkworms with a CD-modified diet for 60 min. It changed from the original yellowish color to blue–white after 90 min of feeding (Figure 5a). After approximately 90 min of feeding, the silk glands showed bright blue–white fluorescence (Figure 5b). This indicated that a large number of CDs had diffused into the glandular lumen of the silk glands from blood. The CD absorption and distribution in silkworm bodies were tentatively demonstrated by the changes in the fluorescence phenomena of tissues using the UVP gel imaging system, which indicated that CDs could quickly and efficiently accumulate in the silk glands, and this change became evident after feeding for 90 min. This is similar to the absorption process of other fluorescent dyes, such as rhodamine B, which is rapidly absorbed by most tissues of the silkworm body, and this change becomes apparent within the first 2 h and saturates within a day [39]. CDs rapidly enter silkworms and accumulate in their blood and silk glands, which allows the feeding cycle to be shortened. This means that to produce fluorescent silks, the silkworms only need to be fed CDs on the sixth day of the fifth instar. Previous research has shown that some dye compounds, such as rhodamine B hexyl ester and acridine orange, were firmly retained without significantly excretion, which caused silkworm death within three days [39]. Thus, we collected silkworm feces after feeding the silkworms a CD-modified diet for 12 h to detect CD excretion from the silkworm. The silkworm feces aqueous extract showed the same blue fluorescence as CD solution under UV light (Figure 5c) and exhibited an intense emission peak centered at 453 nm when exposed to a 370 nm laser (Figure 5d). Therefore, we concluded that the fluorescence of the silkworm feces aqueous extract originated from CDs. The excretion of CDs avoids the toxicity that may result from excessive accumulation.



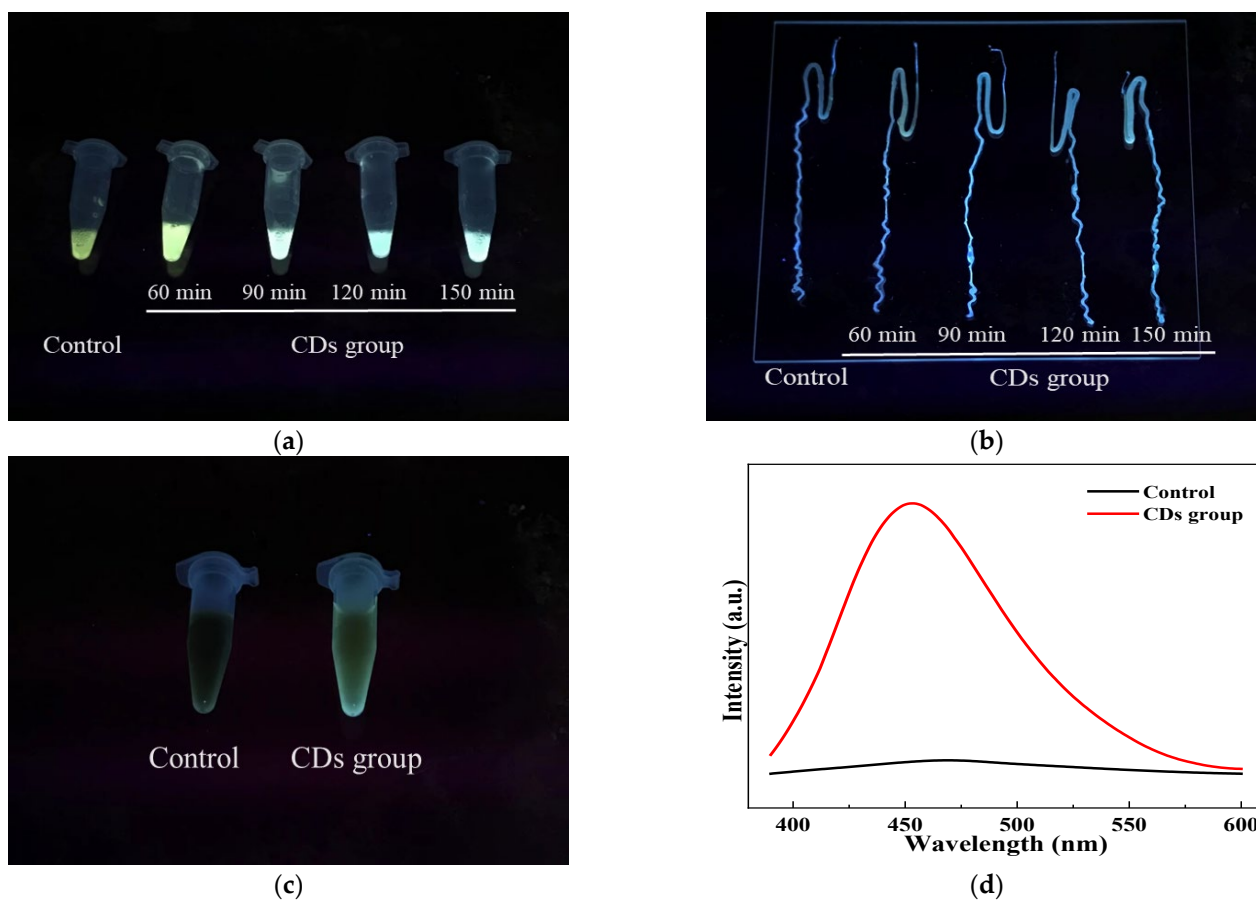


**Figure 5.** Fluorescence images of (a) silkworm blood, (b) silk gland, (c) feces aqueous extract and (d) PL spectra of silkworm feces aqueous extract (measured with an excitation wavelength of 370 nm).

We further investigated the CD distribution in the silk gland under different CD doses. When exposed to UV light, the middle and posterior silk glands of the control group exhibited weak fluorescence, while the silk glands of the CD groups exhibited strong blue–white fluorescence (Figure 6a,b). As the CD mass fraction ratio reached up to 0.50%, the whole silk glands showed bright blue–white fluorescence. The middle and posterior silk glands of the CD groups showed a strong emission peak at 460 nm, the intensity of which increased as the CD dose increased (Figure 6c,d). Only a weak, broad emission peak could be seen in the control group. The fluorescence emission spectra confirmed that the photoluminescence intensity of the posterior silk glands was significantly higher than that of the middle silk glands, illustrating that CDs were most likely located within the posterior silk glands. The fluorescence intensity of the silk glands of the CD groups was dose-dependent. Among them, the CDs-0.75% group had the greatest and most uniform fluorescence intensity. The CDs in this work exhibited an intense emission peak center at 467 nm (Figure 1d). Hence, the fluorescent properties of the silk glands originated from the CDs, and the silkworms could uptake a certain quantity of CD and maintain a certain CD content during the processes of concentration and spinning, causing the modified silk to have an intrinsic blue fluorescence [17]. It has been observed that hydrophilicity, lipophilicity, and the structures created following molecular self-assembly are the factors influencing the distribution of substances in silk [2]. The hydrophilic ligands on the CD surface can interact with the hydrophilic polypeptide chains of sericin and effectively transfer CDs to sericin and fibroin. Therefore, CDs can be distributed in both sericin and fibroin and result in fluorescence.

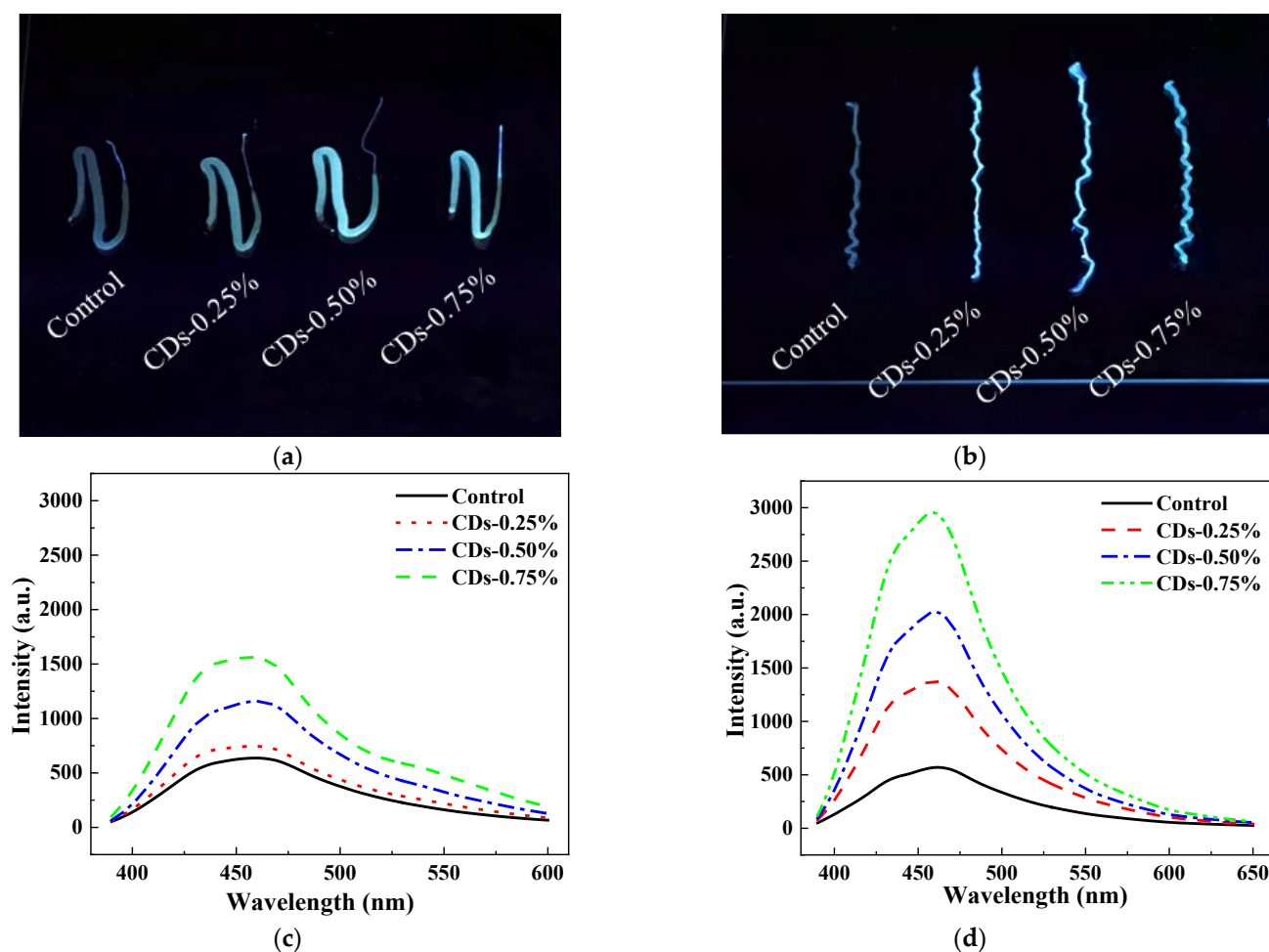


**Figure 6.** Effect of CDs on the fluorescence intensity of silk glands. (a,b) UV pictures of (a) the middle and (b) posterior silk glands. (c,d) PL spectra of (c) the middle and (d) posterior silk glands (measured with an excitation wavelength of 370 nm).

### 3.4. Structure and Properties of Silk Fibroin Fiber

The microscopic morphologies of the control and CD-modified silk fibroin fibers were first compared. Under close magnification in SEM images (Figure 7a–d), the silk fibroin fiber exhibited a similar smooth morphology and had a diameter of approximately 10  $\mu\text{m}$ , illustrating that feeding with CD had no discernible impact on the morphology of the silk. These results may be explained by the CDs' high water dispersibility and small number, which are characteristic differences from graphene,  $\text{TiO}_2$  and other inorganic nanoparticles [40,41]. The fluorescence phenomenon of the silk fibroin fiber was observed at an excitation wavelength of 405 nm by using a confocal laser microscope. A key finding was that just a tiny CD dose could endow the silk with special properties. With the exception of the control group, all silk fibroin fibers displayed an inherent, uniform blue fluorescence at a 405 nm excitation wavelength (Figure 8a–d). In contrast, the silk fibroin fiber of the control group showed weak intrinsic fluorescence. The silk fibroin fiber of the CDs-0.50% group had a better fluorescence performance. The PL spectra (Figure 8e) also demonstrated that the fluorescent intensities of the silk fibroin fibers of the CD groups were more intense than those of the control group. Moreover, we found that excessive CD feeding reduced the fluorescence properties of the silks. In this experiment, as the CD mass fraction increased from 0.50 to 0.75 wt%, the fluorescence intensity of the silk fibroin fiber did not increase but instead decreased. The reason for this may be due to the agglomeration of CDs, which caused a quenching (ACQ) effect [42], leading to silk with a weaker fluorescence. Note that unlike silk fibroin fiber, the silk glands contain a certain amount of water, and the CDs had

a certain dispersion in the silk glands. Thus, the fluorescence performance of silk glands improved with increasing CD mass fraction.

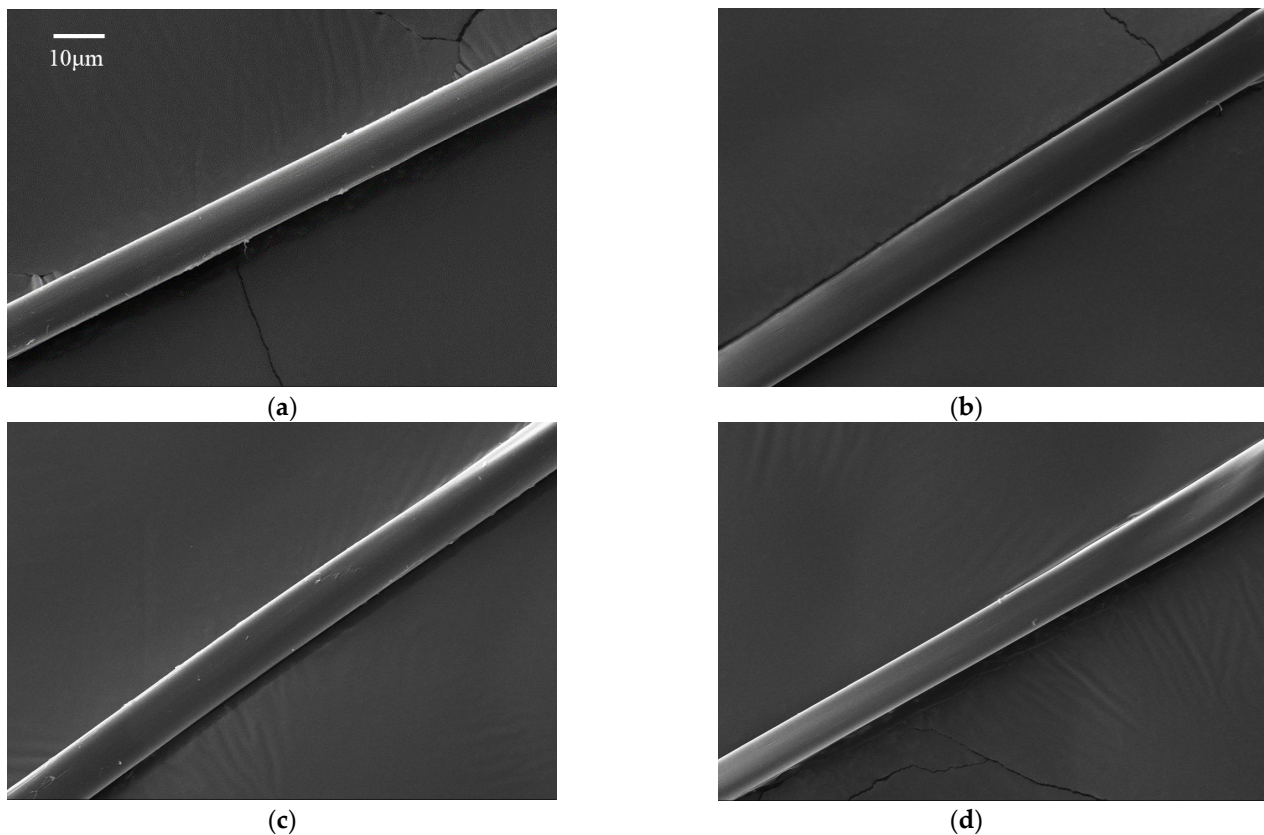


**Figure 7.** SEM images of silk fibroin fiber: (a) control, (b) CDs-0.25%, (c) CDs-0.50% and (d) CDs-0.75%.

Quasi-static tensile tests were conducted on silk fibers to analyze the effect of CDs on the mechanical properties of silkworm silk. The stress–strain curves (Figure 9a) show that the addition of CDs improved the mechanical properties of silk fiber. Among them, the strongest breaking strength was the 28.07 MPa breaking strength of the CDs-0.50% group, which was nearly 1.23 times that of the control group (22.85 MPa), and the elongation at break increased from 21.17 to 22.24%. This indicated that using 0.5% CDs in the diet could effectively enhance the mechanical properties of silk fiber. In addition, this silk fiber was a kind of dual-performance modified silk with intrinsic fluorescence and enhanced mechanical properties. Note that the strain of the silk fiber appears to decrease with increasing CD dose in the range of 0.50–0.75 wt%, which provides a possibility of adjusting the performance of silk fiber for different applications. The modified silks obtained by using a feeding additive can be regarded as a kind of composite in which the silk fibroin was the matrix while the additive, especially the nanoparticle, was the reinforcement. In contrast to organic dyes, such as RhB, Rh110, Rh101 and Rh123, CDs as inorganic nanoparticles have better brightness, and lower toxicity [18]. Therefore, CDs were incorporated in silk fibroin fiber as reinforcement through this in situ approach to produce dual-performance modified silks. In 2019, blue-emitting CDs were first employed in silkworm feed, which produced super strong and intrinsically fluorescent silkworm silk [17]. It is necessary to note that these good functions of modified silk result from a substantial amount of feeding additive. The number of additives in the modified silk should be as few as feasible for bioimaging and other biomedical applications, although these additives have little adverse effect on the growth of silkworms [43]. Moreover, a small dose of additives can reduce the costs of scaling production and avoid any adverse effect of excessive additives on silkworms and

silk fiber. Hence, 0.50 wt% was chosen as the optimum CD dose in this work. This not only ensured a low dosage of additives in the diet but also maintained the best properties of silk while adhering to the principle of sustainable development.

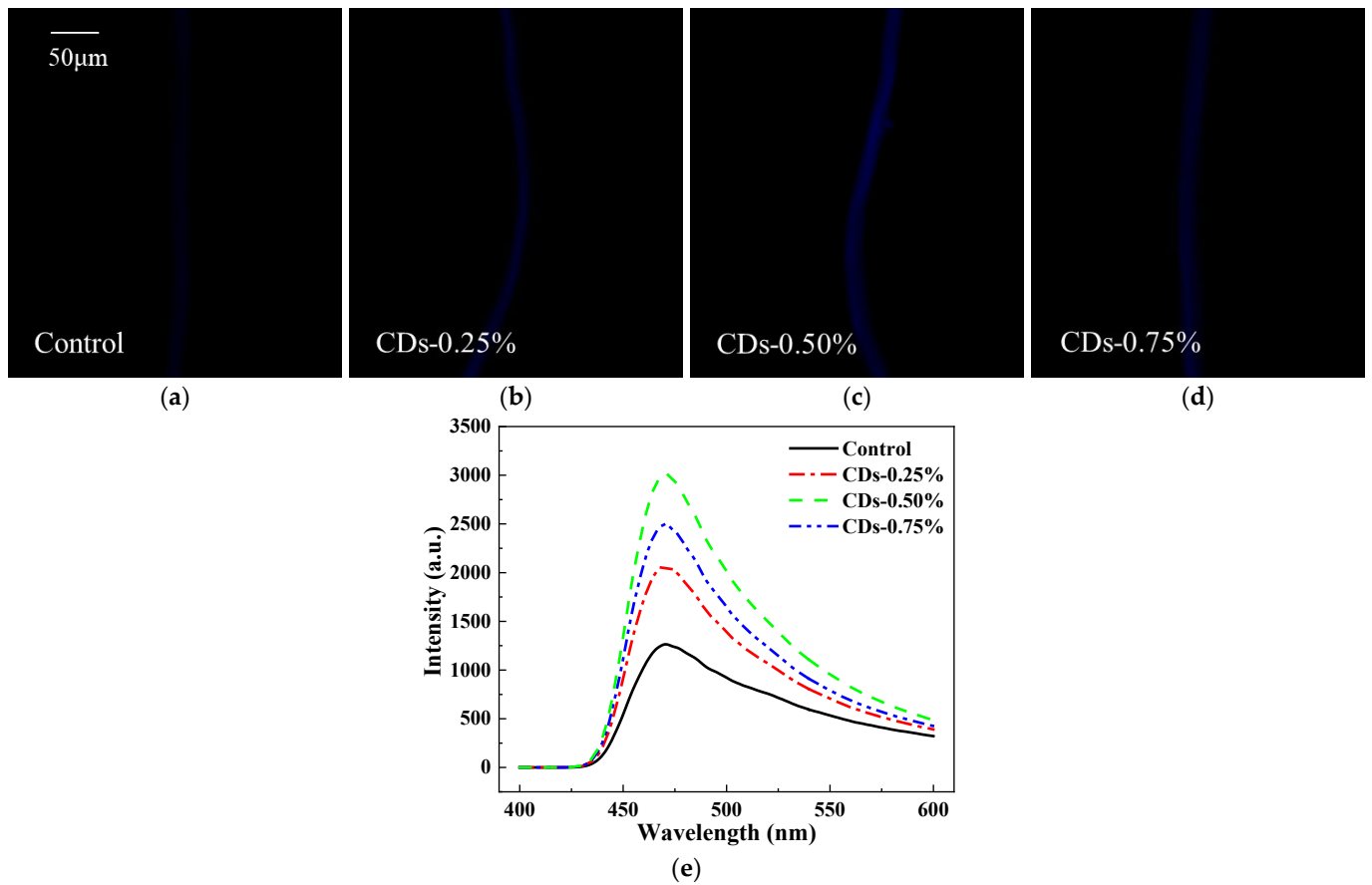


**Figure 8.** Effect of CDs on the fluorescent intensity of silk fibroin fiber. (a–d) Confocal laser microscopy images of silk fibroin fiber (measured with an excitation wavelength of 405 nm); (e) PL spectra of silk fibroin fiber (measured with an excitation wavelength of 370 nm).

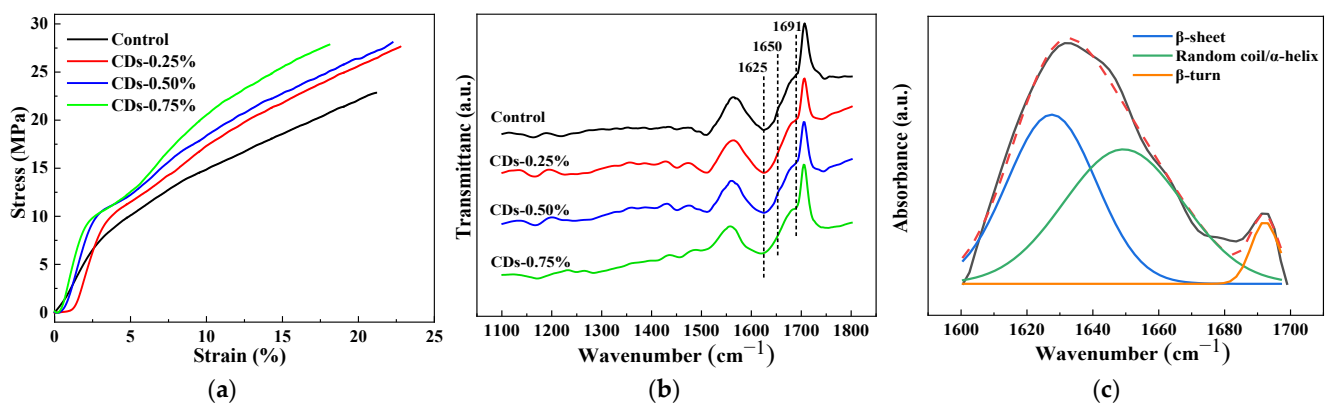


**Figure 9.** Cont.

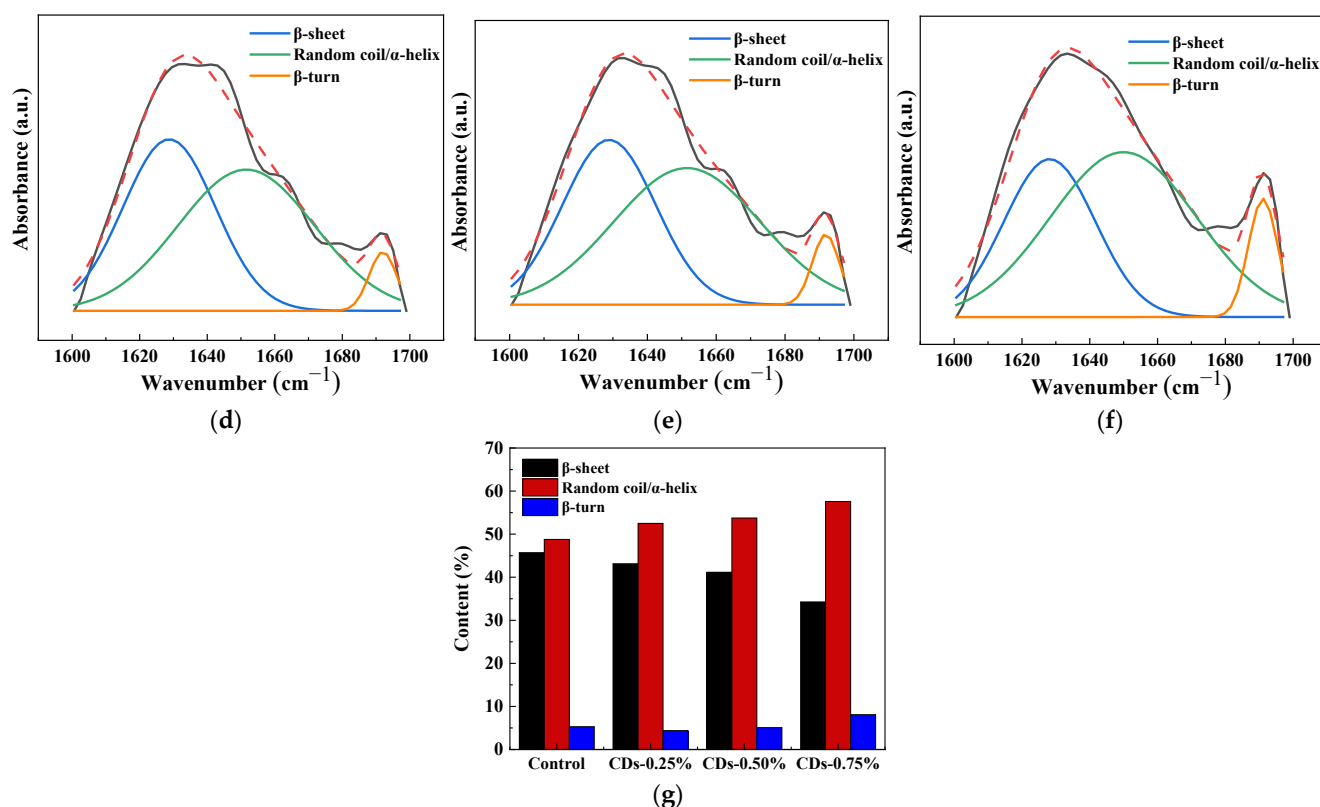


**Figure 9.** Effect of CDs on the mechanical properties of silk fiber. (a) Stress–strain curves of silk fiber; (b) FT-IR spectra of silk fibroin fiber; the deconvolution of FT-IR spectra in the amide I bands of (c) control, (d) CDs-0.25%, (e) CDs-0.50% and (f) CDs-0.75%. (g) Contents of secondary structures obtained based on the amide I bands in FT-IR spectra.

Furthermore, we measured the secondary structures of the silk fibroin fibers, which were connected to mechanical characteristics, by FT-IR. The amide I band (1720–1600 cm<sup>-1</sup>), amide II band (1600–1500 cm<sup>-1</sup>) and amide III band (1350–1200 cm<sup>-1</sup>) were the three primary absorption bands of silk fibroin. The amide I band is most relevant for the study of silk fibroin fiber secondary structures. As shown in Figure 9b, the  $\beta$ -sheet conformation was attributed to the signals at 1625 cm<sup>-1</sup>. The signals at 1650 cm<sup>-1</sup> were attributed to the random coil and  $\alpha$ -helix conformation. The  $\beta$ -turn conformation was attributed to the peak at 1691 cm<sup>-1</sup> [17]. To ascertain the contents of the secondary structures, Fourier self-deconvolution was performed to the amide I region of the silk fibroin fiber (Figure 9c–f); the findings are shown in Figure 9g. Compared with control silk, the CD-modified silk did not have any new characteristic peaks or changes in peak positions, indicating that the addition of CDs did not change the basic structure of silk, but the CD-modified silk contained more chains in random coil/ $\alpha$ -helix conformations and fewer  $\beta$ -sheet conformations. The  $\beta$ -sheet conformations of CD-modified silk decreased by 2.56, 4.54 and 11.43%, respectively, which the random coil/ $\alpha$ -helix conformations increased by 3.72, 4.96 and 8.81%, respectively, compared with the control group. This may be due to the numerous –COOH and –OH groups on the CD surface, which create hydrogen bonds with the amino groups of silk fibroin fibers and hinder the conformational transitions of silk fibroin fibers from random coils/ $\alpha$ -helices to  $\beta$ -sheets. The increased random coil/ $\alpha$ -helix conformation content was beneficial to improve the strain of the silk fibers. When pulled by external force, the flexible fibroin peptide chains of random coil/ $\alpha$ -helix conformation in the amorphous region would deform, firstly. Then, the intensive hydrogen bond interactions causes the CDs to move with protein chains, in turn providing more space for chains to move. This collaborative mobility endowed larger elongation to the modified silk fibers [17]. The creation of CD knots in the fiber due to the formation of hydrogen bonds between the CDs and silk fibroin can improve

the density of the net structure, effectively dispersing outside pressures and showing more significant stress [44]. Furthermore, the CD addition introduced stiff nanomaterials into the silk, further increasing the performance of the modified silk. Interestingly, we observed that the surface of CD-modified silk was smoother and the fibers had fewer flaws than those of the control (Figure 7). Some studies showed that the decreased likelihood of flaws in a fiber could lead to the increase in fiber strength [18]. Based on the above observations, we suggest that the hydrogen bond interactions between the silk fibroin fiber and CDs acted as “cross-linking knots” and hindered the movement of molecular chains, confining the crystallization of the silk fibroin fiber. These factors had a significant part in improving the mechanical properties of the material.

### 3.5. Noncytotoxicity of CD-Modified Silks

Silkworm silk as a natural material has been extensively used as a biological scaffold. The use of fluorescent silk as scaffolds can improve the visualization of tissue scaffolds and the interface between scaffolds and cells for easy monitoring of scaffold function [17]. In this work, we created silk scaffolds by encircling silk fibroin fibers around a coverslip to culture L929 cells (Figure 10). After seeding for 24 and 72 h, the cell morphologies of L929 cells on different substrates were similar. The L929 cells grew well with a clear cell outline and showed spindle-like or flattened morphologies (Figure 11). After staining with DAPI and rhodamine-phalloidin, the L929 cells showed intact nuclei and a clearly structured cytoskeleton (Figure 12). The laser scanning confocal microscopy (LSCM) images further confirmed that the good cytocompatibility of silkworm silks was retained by the CD-modified silks. After 72 h of cell culture, flow cytometry was used to further examine the apoptotic statuses of the L929 cells on silk scaffolds. The results showed that the percentages of viable apoptotic cells on different substrates were all less than 1% (Figure 13a). The percentages of necrotic cells on the coverslip and control silk scaffolds were both less than 1.50%, and that on the CDs-0.50% silk scaffolds was slightly higher at 3.1% (Figure 13b). The percentages of total apoptotic cells on the coverslip, control and CDs-0.50% silk scaffolds were 1.9, 2.1 and 4.0%, respectively (Figure 13c). Finally, the percentages of intact and viable cells on the coverslip, control and CDs-0.50% silk scaffolds were more than 98, 97 and 96%, respectively (Figure 13d), which suggested that CD-modified silks had no cytotoxicity. We further observed the adhesion of L929 cells on the CD-modified silks by SEM. The SEM images showed that a large number of cells adhered to both the control silk scaffolds and CDs-0.50% silk scaffolds after culturing for 72 h (Figure 14). The excellent cytocompatibility and good mechanical properties of the CD-modified silks had a positive impact on cell adhesion and culture, which endowed the modified silks with application potential in tissue engineering. Ultimately, CD-modified silks with good mechanical properties, intrinsically fluorescent properties and excellent biocompatibility might motivate new applications in tissue engineering, fluorescent fabrics and other fields.

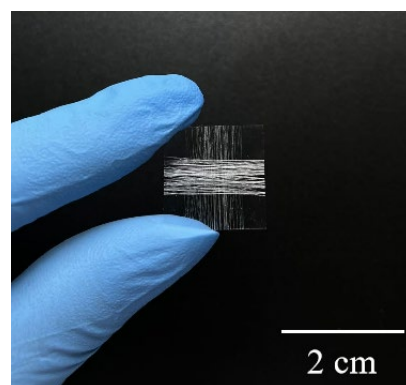


**Figure 10.** Silk scaffolds created by encircling a coverslip with silk fibroin fiber.

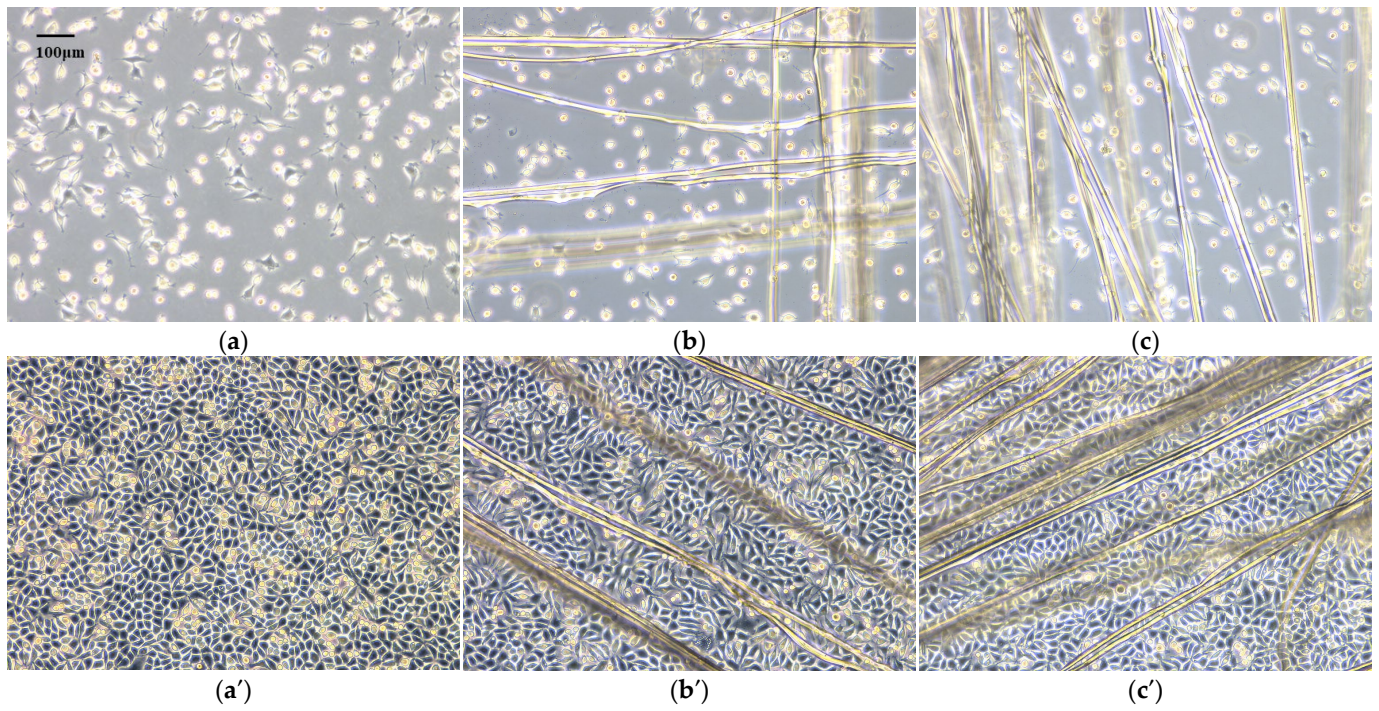


**Figure 11.** Growth and proliferation of L929 cells on silk scaffolds. L929 cells cultured for 24 h on coverslip (a), control (b), and CDs-0.50% silk scaffolds (c); L929 cells cultured for 72 h on coverslip (a'), control (b') and CDs-0.50% silk scaffolds (c').

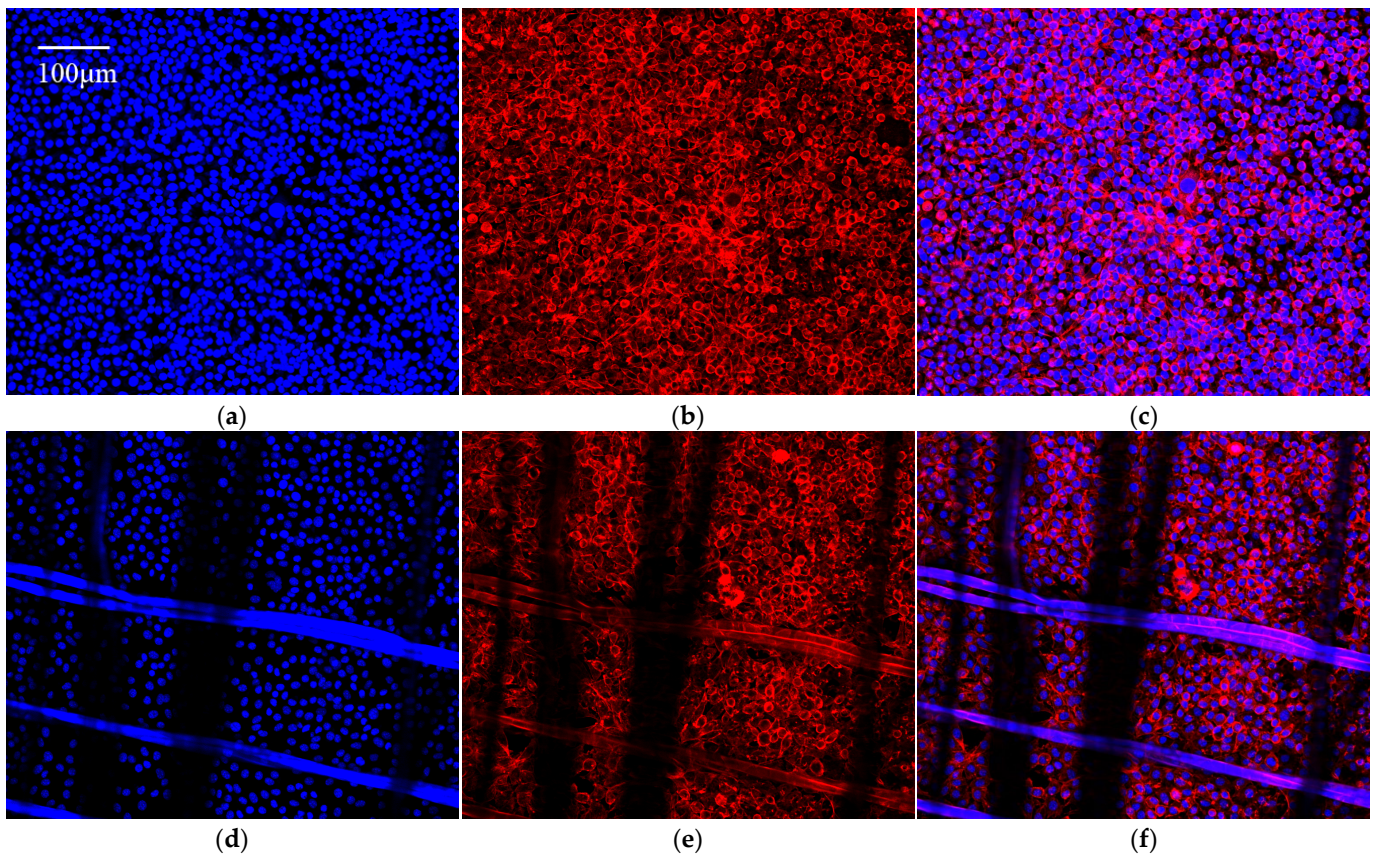


**Figure 12.** Cont.

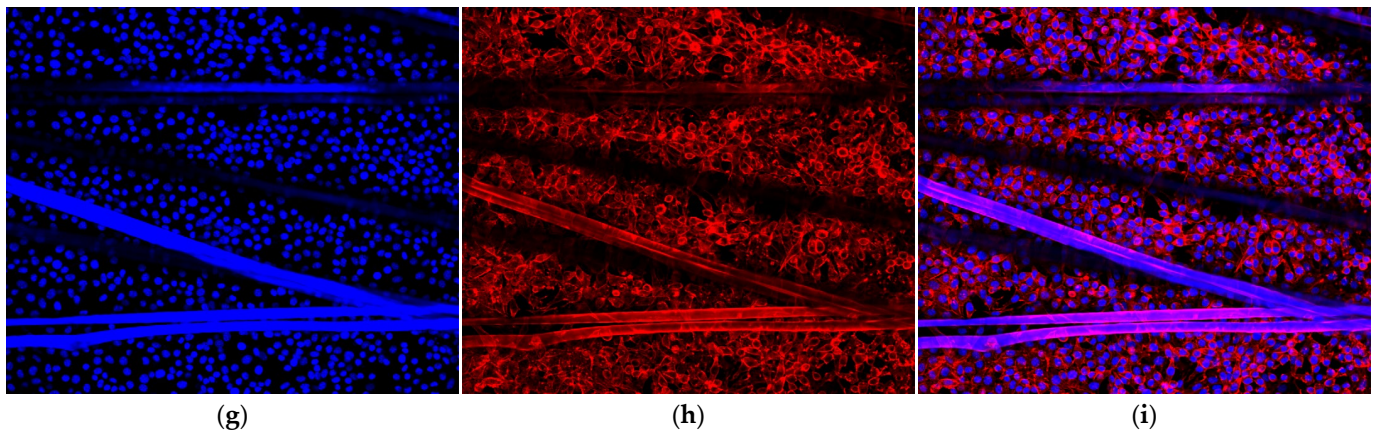


**Figure 12.** LSCM images of L929 cells cultured for 72 h on coverslip (a–c), control (d–f) and CDs-0.50% silk scaffolds (g–i); (a,d,g) L929 cells/silk scaffolds stained with DAPI; (b,e,h) L929 cells/silk scaffolds stained with rhodamine–phalloidin; (c,f,i) L929 cells/silk scaffolds stained with DAPI and rhodamine–phalloidin.

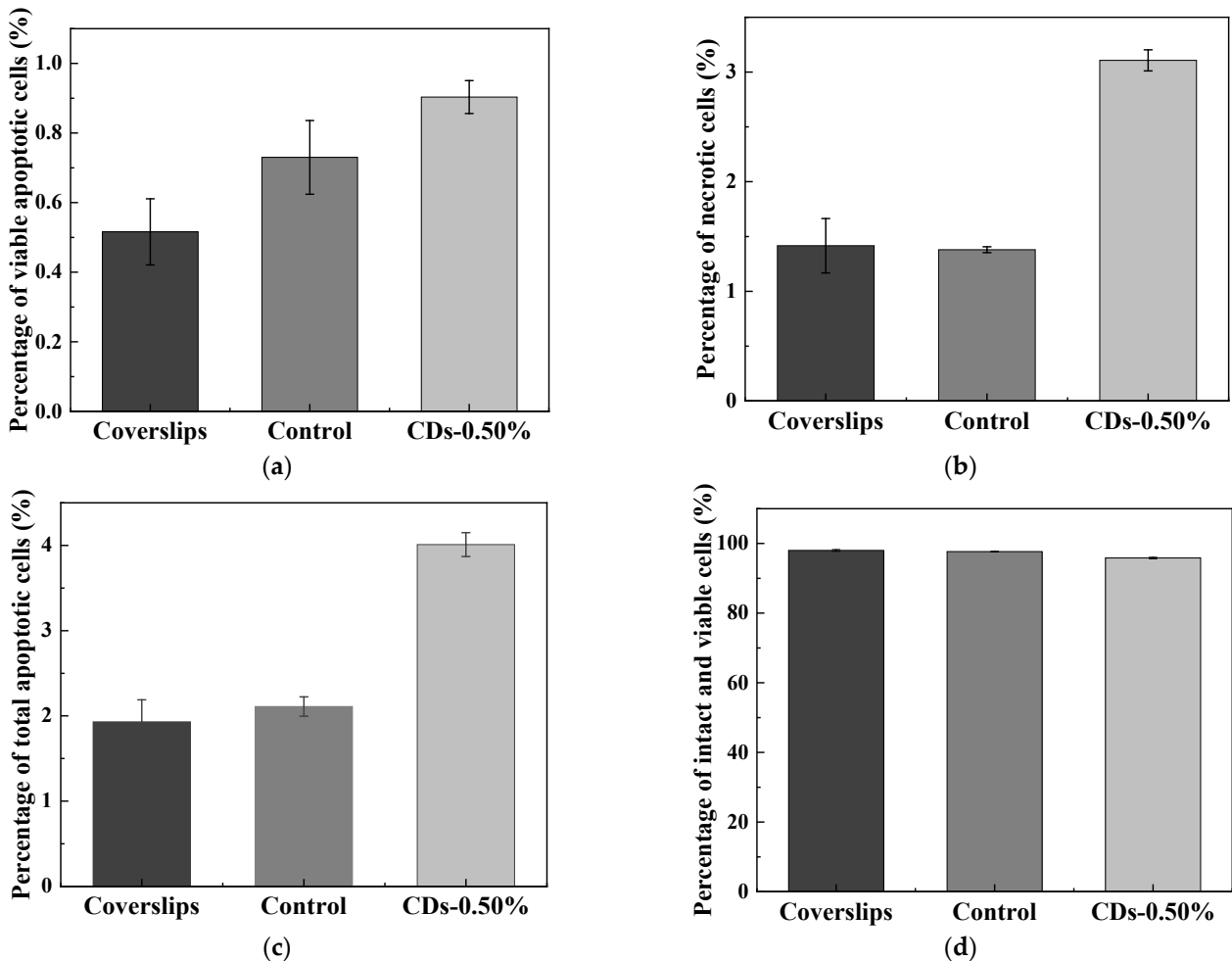


**Figure 13.** Apoptosis of L929 cells on silk scaffolds. (a) Viable apoptotic cells; (b) necrotic cells; (c) total apoptotic cells; (d) intact and viable cells.



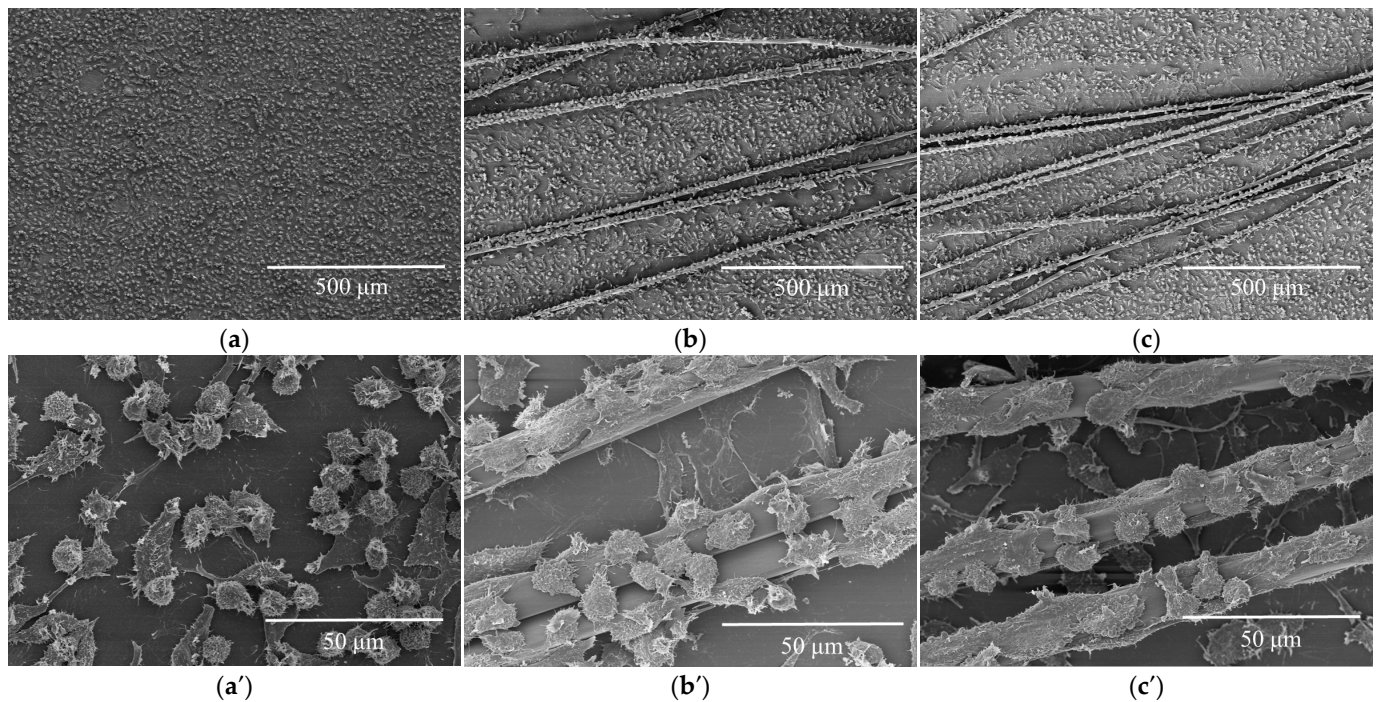


**Figure 14.** SEM images of L929 cells cultured for 72 h on (a,a') coverslip, (b,b') control and (c,c') CDs-0.50% silk scaffolds.

#### 4. Conclusions

The advent of additive feeding strategies provides green and effective methods for manufacturing silk fibers with fluorescent properties. In this work, citric acid and urea were selected as raw materials for synthesizing CDs by microwave-assisted methods. As a result, the synthesized CDs had the advantages of small particle size (approximately 2.8 nm), good dispersion and amphiphilic structure. We fed silkworms with these CDs to fabricate fluorescent silk with enhanced mechanical properties, which was safe for the silkworms and did not affect the silk yield. Compared with ordinary silk, the CDs-0.5%-modified silk displayed intrinsic blue fluorescence when exposed to a 405 nm laser, and the highest elongation at break of this kind of fluorescent silk was 22.24% while the breaking strength was 28.07 MPa, which were increases of 5.05 and 22.84%, respectively. This silk exhibited no cytotoxic effect on L929 cells and had excellent cell adhesion. This study expands our capacity to produce high-quality fluorescent silk on a large scale in a green and sustainable manner.

**Author Contributions:** Conceptualization, W.C.; Y.Z.; G.F.; W.L.; Z.P.; Y.Y.; F.C. and H.Y.; methodology, W.C. and Y.Z.; validation, G.F.; W.L.; Z.P. and Y.Y.; writing—original draft preparation, W.C. and G.F.; writing—review and editing, Y.Z. and F.C.; visualization, W.C. and G.F.; supervision, F.C. and H.Y.; project administration, F.C. and H.Y. funding acquisition, H.Y. All authors have read and agreed to the published version of the manuscript.

**Funding:** This study was financially supported by Guangdong Modern Agricultural Industry Technology System (Grant No. 2022KJ124); Guangdong Provincial Key R&D Programme (Grant No. 2020B020225005).

**Institutional Review Board Statement:** Not applicable.

**Informed Consent Statement:** Not applicable.

**Data Availability Statement:** Not applicable.

**Conflicts of Interest:** The authors declare no conflict of interest.

## References

1. Wang, C.; Xia, K.; Zhang, Y.; Kaplan, D.L. Silk-Based Advanced Materials for Soft Electronics. *Acc. Chem. Res.* **2019**, *52*, 2916–2927. [[CrossRef](#)]
2. Tansil, N.C.; Koh, L.D.; Han, M.Y. Functional Silk: Colored and Luminescent. *Adv. Mater.* **2012**, *24*, 1350. [[CrossRef](#)]
3. Nisal, A.; Trivedy, K.; Mohammad, H.; Panneri, S.; Sen Gupta, S.; Lele, A.; Manchala, R.; Kumar, N.S.; Gadgil, M.; Khandelwal, H.; et al. Uptake of Azo Dyes into Silk Glands for Production of Colored Silk Cocoons Using a Green Feeding Approach. *ACS Sustain. Chem. Eng.* **2014**, *2*, 312–317. [[CrossRef](#)]
4. Kim, D.W.; Lee, O.J.; Kim, S.-W.; Ki, C.S.; Chao, J.R.; Yoo, H.; Yoon, S.-i.; Lee, J.E.; Park, Y.R.; Kweon, H.; et al. Novel fabrication of fluorescent silk utilized in biotechnological and medical applications. *Biomaterials* **2015**, *70*, 48–56. [[CrossRef](#)]
5. Zhou, Z.; Shi, Z.; Cai, X.; Zhang, S.; Corder, S.G.; Li, X.; Zhang, Y.; Zhang, G.; Chen, L.; Liu, M.; et al. The Use of Functionalized Silk Fibroin Films as a Platform for Optical Diffraction-Based Sensing Applications. *Adv. Mater.* **2017**, *29*, 1605471. [[CrossRef](#)]
6. Wang, Q.; Jian, M.; Wang, C.; Zhang, Y. Carbonized Silk Nanofiber Membrane for Transparent and Sensitive Electronic Skin. *Adv. Funct. Mater.* **2017**, *27*, 1605657. [[CrossRef](#)]
7. Koh, L.-D.; Cheng, Y.; Teng, C.-P.; Khin, Y.-W.; Loh, X.-J.; Tee, S.-Y.; Low, M.; Ye, E.; Yu, H.-D.; Zhang, Y.-W.; et al. Structures, mechanical properties and applications of silk fibroin materials. *Prog. Polym. Sci.* **2015**, *46*, 86–110. [[CrossRef](#)]
8. Meng, M.; He, H.; Xiao, J.; Zhao, P.; Xie, J.; Lu, Z. Controllable in situ synthesis of silver nanoparticles on multilayered film-coated silk fibers for antibacterial application. *J. Colloid Interface Sci.* **2016**, *461*, 369–375. [[CrossRef](#)] [[PubMed](#)]
9. Min, K.; Kim, S.; Kim, C.G.; Kim, S. Colored and fluorescent nanofibrous silk as a physically transient chemosensor and vitamin deliverer. *Sci. Rep.* **2017**, *7*, 5448. [[CrossRef](#)]
10. Lu, D.; Zheng, Z.; Guo, S.; Wang, C.; Kaplan, D.L.; Wang, X. Binding Quantum Dots to Silk Biomaterials for Optical Sensing. *J. Sens.* **2015**, *2015*, 819373. [[CrossRef](#)]
11. Zheng, Z.Z.; Liu, M.; Guo, S.Z.; Wu, J.B.; Lu, D.S.; Li, G.; Liu, S.S.; Wang, X.Q.; Kaplan, D.L. Incorporation of quantum dots into silk biomaterials for fluorescence imaging. *J. Mater. Chem. B* **2015**, *3*, 6509–6519. [[CrossRef](#)]
12. Zhang, P.; Lan, J.; Wang, Y.; Xiong, Z.H.; Huang, C.Z. Luminescent golden silk and fabric through in situ chemically coating pristine-silk with gold nanoclusters. *Biomaterials* **2015**, *36*, 26–32. [[CrossRef](#)] [[PubMed](#)]
13. Tang, B.; Li, J.; Hou, X.; Afrin, T.; Sun, L.; Wang, X. Colorful and Antibacterial Silk Fiber from Anisotropic Silver Nanoparticles. *Ind. Eng. Chem. Res.* **2013**, *52*, 4556–4563. [[CrossRef](#)]
14. Ali, N.; El-Khatib, E.; El-Mohamedy, R.; Ramadan, M. Antimicrobial activity of silk fabrics dyed with saffron dye using microwave heating. *Int. J. Curr. Microbiol. Appl. Sci.* **2014**, *3*, 140–146.
15. Chen, W.; Wang, Z.; Cui, Z.; Meng, Z.; Huang, M.; Pan, D. Study on coloration of silk based on coupling reaction with a diazonium compound. *Fibers Polym.* **2014**, *15*, 966–970. [[CrossRef](#)]
16. Kim, S.W.; Yun, E.Y.; Choi, K.-H.; Kim, S.R.; Park, S.W.; Kang, S.W.; Kwon, O.-Y.; Goo, T.W. Construction of fluorescent red silk using fibroin H-chain expression system. *J. Sericultural Entomol. Sci.* **2012**, *50*, 87–92. [[CrossRef](#)]
17. Fan, S.; Zheng, X.; Zhan, Q.; Zhang, H.; Shao, H.; Wang, J.; Cao, C.; Zhu, M.; Wang, D.; Zhang, Y. Super-strong and intrinsically fluorescent silkworm silk from carbon nanodots feeding. *Nano Micro Lett.* **2019**, *11*, 75. [[CrossRef](#)]
18. Cheng, L.; Zhao, H.; Huang, H.; Li, B.; Li, R.K.Y.; Feng, X.-Q.; Dai, F. Quantum dots-reinforced luminescent silkworm silk with superior mechanical properties and highly stable fluorescence. *J. Mater. Sci.* **2019**, *54*, 9945–9957. [[CrossRef](#)]
19. Wu, S.; Weng, P.; Tang, Z.; Guo, B. Sustainable Carbon Nanodots with Tunable Radical Scavenging Activity for Elastomers. *ACS Sustain. Chem. Eng.* **2016**, *4*, 247–254. [[CrossRef](#)]
20. Meng, W.; Bai, X.; Wang, B.; Liu, Z.; Lu, S.; Yang, B. Biomass-Derived Carbon Dots and Their Applications. *Energy Environ. Mater.* **2019**, *2*, 172–192. [[CrossRef](#)]
21. Liu, J.; Kong, T.; Xiong, H.-M. Mulberry-Leaves-Derived Red-Emissive Carbon Dots for Feeding Silkworms to Produce Brightly Fluorescent Silk. *Adv. Mater.* **2022**, *34*, 2200152. [[CrossRef](#)] [[PubMed](#)]
22. Wang, D.; Wang, Z.; Zhan, Q.; Pu, Y.; Wang, J.-X.; Foster, N.R.; Dai, L. Facile and Scalable Preparation of Fluorescent Carbon Dots for Multifunctional Applications. *Engineering* **2017**, *3*, 402–408. [[CrossRef](#)]
23. de Medeiros, T.V.; Manioudakis, J.; Noun, F.; Macairan, J.-R.; Victoria, F.; Naccache, R. Microwave-assisted synthesis of carbon dots and their applications. *J. Mater. Chem. C* **2019**, *7*, 7175–7195. [[CrossRef](#)]
24. Wang, X.; Qu, K.; Xu, B.; Ren, J.; Qu, X. Microwave assisted one-step green synthesis of cell-permeable multicolor photoluminescent carbon dots without surface passivation reagents. *J. Mater. Chem.* **2011**, *21*, 2445–2450. [[CrossRef](#)]
25. Zhao, H.-P.; Feng, X.-Q.; Shi, H.-J. Variability in mechanical properties of *Bombyx mori* silk. *Mater. Sci. Eng. C* **2007**, *27*, 675–683. [[CrossRef](#)]
26. Ling, S.; Qi, Z.; Knight, D.P.; Shao, Z.; Chen, X. Synchrotron FTIR Microspectroscopy of Single Natural Silk Fibers. *Biomacromolecules* **2011**, *12*, 3344–3349. [[CrossRef](#)]
27. Peng, J.; Gao, W.; Gupta, B.K.; Liu, Z.; Romero-Aburto, R.; Ge, L.; Song, L.; Alemany, L.B.; Zhan, X.; Gao, G.; et al. Graphene Quantum Dots Derived from Carbon Fibers. *Nano Lett.* **2012**, *12*, 844–849. [[CrossRef](#)]
28. Zhu, S.; Zhang, J.; Tang, S.; Qiao, C.; Wang, L.; Wang, H.; Liu, X.; Li, B.; Li, Y.; Yu, W.; et al. Surface Chemistry Routes to Modulate the Photoluminescence of Graphene Quantum Dots: From Fluorescence Mechanism to Up-Conversion Bioimaging Applications. *Adv. Funct. Mater.* **2012**, *22*, 4732–4740. [[CrossRef](#)]

29. Das, B.; Dadhich, P.; Pal, P.; Srivas, P.K.; Bankoti, K.; Dhara, S. Carbon nanodots from date molasses: New nanolights for the in vitro scavenging of reactive oxygen species. *J. Mater. Chem. B* **2014**, *2*, 6839–6847. [[CrossRef](#)] [[PubMed](#)]
30. Zhang, W.; Shi, L.; Liu, Y.; Meng, X.; Xu, H.; Xu, Y.; Liu, B.; Fang, X.; Li, H.-B.; Ding, T. Supramolecular interactions via hydrogen bonding contributing to citric-acid derived carbon dots with high quantum yield and sensitive photoluminescence. *RSC Adv.* **2017**, *7*, 20345–20353. [[CrossRef](#)]
31. Zhu, W.; Meng, X.; Li, H.; He, F.; Wang, L.; Xu, H.; Huang, Y.; Zhang, W.; Fang, X.; Ding, T. Ethanothermal synthesis of phenol-derived carbon dots with multiple color emission via a versatile oxidation strategy. *Opt. Mater.* **2019**, *88*, 412–416. [[CrossRef](#)]
32. Yoshinaga, T.; Iso, Y.; Isobe, T. Particulate, Structural, and Optical Properties of D-Glucose-Derived Carbon Dots Synthesized by Microwave-Assisted Hydrothermal Treatment. *ECS J. Solid State Sci. Technol.* **2017**, *7*, R3034–R3039. [[CrossRef](#)]
33. Cheng, L.; Huang, H.; Chen, S.; Wang, W.; Dai, F.; Zhao, H. Characterization of silkworm larvae growth and properties of silk fibres after direct feeding of copper or silver nanoparticles. *Mater. Des.* **2017**, *129*, 125–134. [[CrossRef](#)]
34. Santorum, M.; Costa, R.M.; dos Reis, G.H.; Carvalho dos Santos, D. Novaluron impairs the silk gland and productive performance of silkworm *Bombyx mori* (Lepidoptera: Bombycidae) larvae. *Chemosphere* **2020**, *239*, 124697. [[CrossRef](#)] [[PubMed](#)]
35. Li, B.; Yu, X.; Gui, S.; Xie, Y.; Hong, J.; Zhao, X.; Sheng, L.; Sang, X.; Sun, Q.; Wang, L.; et al. Titanium Dioxide Nanoparticles Relieve Silk Gland Damage and Increase Cocooning of *Bombyx mori* under Phoxim-Induced Toxicity. *J. Agric. Food Chem.* **2013**, *61*, 12238–12243. [[CrossRef](#)] [[PubMed](#)]
36. Walkey, C.D.; Chan, W.C.W. Understanding and controlling the interaction of nanomaterials with proteins in a physiological environment. *Chem. Soc. Rev.* **2012**, *41*, 2780–2799. [[CrossRef](#)]
37. Chiti, F.; Dobson, C.M. Protein misfolding, functional amyloid, and human disease. *Annu. Rev. Biochem.* **2006**, *75*, 333–366. [[CrossRef](#)]
38. Dong, H.; Bi, Y.; Wang, J.-L.; Liu, Y.-Q.; Wang, H. Safety evaluation of four entomopathogenic nematode species against two silkworm species. *Entomol. Res.* **2020**, *50*, 155–162. [[CrossRef](#)]
39. Tansil, N.C.; Li, Y.; Koh, L.D.; Peng, T.C.; Win, K.Y.; Liu, X.Y.; Han, M.-Y. The use of molecular fluorescent markers to monitor absorption and distribution of xenobiotics in a silkworm model. *Biomaterials* **2011**, *32*, 9576–9583. [[CrossRef](#)]
40. Cai, L.; Shao, H.; Hu, X.; Zhang, Y. Reinforced and Ultraviolet Resistant Silks from Silkworms Fed with Titanium Dioxide Nanoparticles. *ACS Sustain. Chem. Eng.* **2015**, *3*, 2551–2557. [[CrossRef](#)]
41. Wang, Q.; Wang, C.; Zhang, M.; Jian, M.; Zhang, Y. Feeding Single-Walled Carbon Nanotubes or Graphene to Silkworms for Reinforced Silk Fibers. *Nano Lett.* **2016**, *16*, 6695–6700. [[CrossRef](#)] [[PubMed](#)]
42. Zhang, L.; Zhang, Z.-Y.; Liang, R.-P.; Li, Y.-H.; Qiu, J.-D. Boron-Doped Graphene Quantum Dots for Selective Glucose Sensing Based on the “Abnormal” Aggregation-Induced Photoluminescence Enhancement. *Anal. Chem.* **2014**, *86*, 4423–4430. [[CrossRef](#)] [[PubMed](#)]
43. Zhan, Q.; Fan, S.; Wang, D.; Yao, X.; Shao, H.; Zhang, Y. Super-strong and uniform fluorescent composite silk from trace AIE nanoparticle feeding. *Compos. Commun.* **2020**, *21*, 100414. [[CrossRef](#)]
44. Li, J.; Li, Y.; Lu, S.; Zhang, J.; Zhang, C.; Xiong, L. Dual-Performance Optimized Silks from Ultra-Low Dose Polymer Dots Feeding and Its Absorption, Distribution and Excretion in the Silkworms. *Adv. Fiber Mater.* **2022**, *4*, 845–858. [[CrossRef](#)]

**Disclaimer/Publisher’s Note:** The statements, opinions and data contained in all publications are solely those of the individual author(s) and contributor(s) and not of MDPI and/or the editor(s). MDPI and/or the editor(s) disclaim responsibility for any injury to people or property resulting from any ideas, methods, instructions or products referred to in the content.